The Journal of Immunology, 2026, 215(11), vkag295
https://doi.org/10.1093/jimmun/vkag295
Cutting Edge

Interleukin-15 complex–induced interleukin-10 acts on brain endothelial cells to reduce CD8 T-cell arrest during cerebral malaria

Jacob A. Hildebrand[1,2], Erin D. Lucas[1,2], Noah R. Daniels[1,2], Benjamin D. Fisher[1,2], Chris J. Janse[3], Kory R. Johnson[4], Caleb Y. Kim[1], Jason S. Mitchell[1,5], Jules A. Sangala[1,6], Trevor N. Tankersley[1,2], Brian T. Fife[1,5], Dorian B. McGavern[7,*], Geoffrey T. Hart[1,6,*], and Sara E. Hamilton[1,2,*]

[1]Center for Immunology, University of Minnesota, Minneapolis, MN, United States
[2]Department of Laboratory Medicine and Pathology, University of Minnesota, Minneapolis, MN, United States
[3]Leiden University Centre for Infectious Diseases, Leiden University Medical Center, Leiden, The Netherlands
[4]Bioinformatics Core, Division of Intramural Research, National Institutes of Health, Bethesda, MD, United States
[5]Division of Rheumatic and Autoimmune Diseases, Department of Medicine, University of Minnesota, Minneapolis, MN, United States
[6]Division of Infectious Disease and International Medicine, Department of Medicine, University of Minnesota, Minneapolis, MN, United States
[7]Viral Immunology and Intravital Imaging Section, National Institute of Neurological Disorders and Stroke, National Institutes of Health, Bethesda, MD, United States
*Corresponding authors: Sara E. Hamilton, Center for Immunology, Department of Laboratory Medicine and Pathology, University of Minnesota, Wallin Medical Biosciences Bldg, 2101 6th St. SE, Minneapolis, MN 55455, United States. Email: hamil062@umn.edu and Geoffrey T. Hart, Center for Immunology, Department of Medicine, Division of Infectious Disease and International Medicine, University of Minnesota, 4-125 Cancer and Cardiovascular Research Building, 2231 6th St. SE, Minneapolis, MN 55455, United States. Email: hart0792@umn.edu

Abstract

Cerebral malaria (CM) is a life-threatening complication of *Plasmodium* infection driven in part by an overwhelming inflammatory response. No clinical therapies are approved that specifically prevent immunopathology during CM. In experimental cerebral malaria (ECM), vascular endothelial cells in the mouse brain cross-present malaria antigen and upregulate adhesion molecules in response to inflammation. This causes CD8 T-cell arrest, activation, and lethal disruption of the blood-brain barrier. We previously reported that treatment with IL-15 cytokine complex (IL-15C) prevents ECM by inducing natural killer (NK) cell secretion of IL-10. To further uncover the mechanisms underlying this immunotherapy, OT-I T cells were transferred into mice, followed by infection with ovalbumin-expressing *Plasmodium berghei*. Using intravital microscopy, we observed major areas of OT-I arrest within the brains of untreated mice experiencing ECM. IL-15C treatment reduced the number of arresting OT-I T cells, coinciding with an increased mean velocity when compared to untreated mice. To identify the target of NK cell–secreted IL-10, we used conditional knockouts of IL-10Rα and found that protection from ECM occurs through IL-10Rα on endothelial cells and not CD8 T cells. Coinciding with this, IL-15C reduced the expression of adhesion molecules, selectins, and MHC-I on brain endothelial cells. In summary, our studies support the mechanism that IL-15C treatment reduces the number of arrested CD8 T cells along the cerebral vasculature by modulating endothelial cells to prevent ECM. These insights demonstrate the potential for treatments that reduce T-cell arrest to improve outcomes of human CM.

Keywords CD8 T cells, cerebral malaria, intravital microscopy, *Plasmodium*, T-cell arrest

Introduction

Malaria infection is a major global health burden, causing more than 280 million cases annually.[1] The malaria life cycle occurs in multiple stages, with an initial period of hepatocyte invasion followed by release of parasites into the blood. During the blood stage of malaria, individuals without clinical immunity develop a febrile illness with the potential to progress into severe disease. Cerebral malaria (CM) is the deadliest complication of *Plasmodium* infection, causing more than 600,000 deaths per year, primarily in African children <5 years of age.[1,2] These complications result from sequestration of infected red blood cells (RBCs) within tissues, alongside a hyperinflammatory immune response.[2] Current clinical practices alleviate symptoms by clearing the parasite with antimalarial treatments.[3] However, drug-resistant parasite strains have become increasingly

Received: November 4, 2025. **Revised:** October 2, 2026. **Accepted:** October 12, 2026
© The Author(s) 2026. Published by Oxford University Press on behalf of The American Association of Immunologists.
This is an Open Access article distributed under the terms of the Creative Commons Attribution-NonCommercial License (https://creativecommons.org/licenses/by-nc/4.0/), which permits non-commercial re-use, distribution, and reproduction in any medium, provided the original work is properly cited. For commercial re-use, please contact reprints@oup.com for reprints and translation rights for reprints. All other permissions can be obtained through our RightsLink service via the Permissions link on the article page on our site—for further information please contact journals.permissions@oup.com.

common,[4] and no adjunctive therapies exist that modulate the immune response to malaria.

The murine model of experimental cerebral malaria (ECM) has highlighted CD8 T cells as the primary culprit driving immunopathology in the mouse brain during infection with *Plasmodium berghei* ANKA (PbA). Malaria-infected RBCs adhere to the vascular endothelium to avoid immune detection and filtration within the spleen.[5] In response to local IFN-γ production, endothelial cells secrete chemoattractants, upregulate surface expression of cellular adhesion molecules (eg selectins, VCAMs, and ICAMs), and cross-present malaria peptides on their surface.[6–8] CD8 T cells then arrest along the vasculature, recognize their cognate antigen, and secrete effector molecules such as IFN-γ,[7,9] perforin,[10,11] and granzyme B.[12] This disrupts tight junction proteins between endothelial cells, causing severe brain edema, hemorrhaging, and death in most mice.[7,10] In humans, granzyme B–expressing CD8 T cells accumulate in postmortem brains of children who succumbed to disease,[13] suggesting shared features between ECM and human disease. Given the increasing evidence that CD8 T cells are key drivers of cerebral disease, it is critical to find interventions that can restrict their immunopathology.

Natural killer (NK) cells are primarily known for their ability to recognize and lyse transformed cells either during viral infection or cancer.[14] Contemporary research has found that they can also regulate immune responses in a variety of settings.[15] NK cell regulation of the immune response to malaria could occur either through direct lysis of a target cell or by production of immunosuppressive cytokines.[16] Previous work by our lab defined a novel role for IL-10–producing NK cells during ECM. Treatment with IL-15 cytokine complex (IL-15C; IL-15 cytokine combined with a soluble form of IL-15Rα) accelerated the production of IL-10 by NK cells and was sufficient to rescue mice from otherwise lethal disease in an NK cell–derived IL-10–dependent manner.[17] To show this, IL-15C–stimulated wild-type (WT) NK cells were adoptively transferred into PbA-infected mice, which limited ECM, whereas this effect was lost when IL-15C–stimulated IL-$10^{-/-}$ NK cells were transferred instead. Additional work from our group found that NK cells from malaria-experienced adults who are exposed to *Plasmodium* infection but do not develop cerebral disease produce higher levels of IL-10 than malaria-naïve controls.[18] These studies suggest that NK cell–derived IL-10 may be a protective mechanism to limit inflammation in both mice and humans. However, the precise mechanisms by which IL-15C prevents immunopathology during ECM are still unclear.

Here, we further investigate the mechanisms by which IL-15C treatment modulates the acute immune response during ECM. Using a transgenic ovalbumin (OVA)–expressing PbA parasite, we characterized both endogenous and transgenic CD8 T cells in the brain during ECM. We found that while CD8 T-cell migration to the brain is similar between untreated and treated mice, IL-15C treatment reduces the frequency of CD8 T cells expressing granzyme B in the blood and brain. We also employed multiphoton microscopy to study cellular interactions in the brain in vivo, revealing significant areas of CD8 T-cell arrest in untreated mice experiencing ECM. IL-15C treatment reduced the number of arrested CD8 T cells in the brain. IL-15C also reduced the arrest of NK cells in the brain, suggesting similar migration programs between CD8 T cells and NK cells in the cerebral vasculature. We did not observe any sustained interactions between CD8 T cells and NK cells, and loss of IL-10 receptor alpha chain (IL-10Rα) on CD8 T cells did not abolish the protection afforded by treatment, supporting an indirect method of IL-10 regulation. Instead, we find that protection afforded by NK cell–secreted IL-10 acts through IL-10Rα on endothelial cells. We show that IL-15C treatment reduces brain endothelial cell expression of surface receptors that influence T-cell activation and arrest, including adhesion molecules, selectins, and MHC-I. Finally, loss of IL-10Rα on endothelial cells reduced IL-15C–mediated protection from ECM. Our data support a model in which IL-15C treatment inhibits endothelial cell activation during ECM, thus reducing T-cell arrest, activation, and vascular damage.

Materials and methods

Ethics statement

Mice were housed at the University of Minnesota (Minneapolis, MN) and studies were carried out under the Institutional Animal Care and Use Committee (IACUC). The health of uninfected animals was monitored daily, and mice infected with PbA were monitored at least twice per day between day 5 and day 10 post-infection (p.i.).

Mice

All strains used in this work are on the C57BL/6 background. OT-I donor mice[19] were crossed to either C57BL/6-Ly5.1 mice[20] (Charles River Laboratories) or ubiquitin C –green fluorescent protein (GFP) transgenic mice.[21] VE-cadherin^{CreERT2} mice[22] and Ncr1^{iCre} mice[23] were crossed to Ai14 mice,[24] obtained from The Jackson Laboratory. CD8^{Cre} mice[25] were crossed with IL-10Rα$^{fl/fl}$ mice,[26] both obtained from The Jackson Laboratory. All experimental mice, both male and female, were 6 to 10 weeks old on the date of infection. All mice were housed in specific pathogen–free conditions and bred following all IACUC procedures at the University of Minnesota.

Plasmodium infections and monitoring of infected mice

Plasmodium berghei ANKA WT parasites[27] (Dr. Geoffrey Hart, University of Minnesota) and transgenic *P. berghei* ANKA parasites expressing mCherry-OVA[28] (obtained from Dr. Chris Janse, Leiden University Medical Center, Leiden, the Netherlands) were passaged in C57BL/6 mice prior to cryopreservation. Donor mice were infected with 10^6 infected RBCs, delivered by retro-orbital injection (i.v.). On day 6 to 7 p.i. (parasitemia ∼5%), blood from donor mice was diluted 1:2 in Alsever's solution containing 10% glycerol, then snap-frozen in cryovials on dry ice. Vials were then transferred to liquid nitrogen for long-term storage.

On the day of infection, a vial of PbA-WT or PbA-OVA was thawed, and 10^6 infected RBCs were diluted in PBS before retro-orbital injection (i.v.) into experimental mice. Parasitemia was measured by flow cytometry as previously described,[29] determined as the percentage of RBCs (Ter119$^+$CD45$^-$) that stained positive for DNA and RNA. Between days 5 and 10 p.i., PbA-

infected mice were checked twice per day for the development of symptoms associated with CM. To determine the severity of disease, a modified version of the SNAP scoring system was used.[30] Mice were scored between 0 and 2 points based on their grip strength, visual placement, reflexes, gait, and balance. A mouse with a score >6 was considered moribund.

Adoptive transfer of transgenic OT-I T cells

Spleens were taken from donor OT-I (CD45.1$^+$ or GFP$^+$) mice and mashed through 70-μm strainers. Cells were briefly incubated at room temperature in RBC lysis solution before washing with RPMI supplemented with 5% FBS. CD8 T cells were enriched using the Mojosort Mouse CD8 T Cell Isolation Kit (BioLegend) and collected from the unbound fraction. Enriched CD8 T cells were counted, and a small aliquot was prepared for flow cytometry by staining with anti-CD8α and anti-Vα2 to determine purity. Cell counts were then adjusted to 5×10^5 cells/mL in PBS, followed by injection (i.v.) of 100 μL of cell suspension into experimental mice.

Intravascular staining

Intravascular staining of cells for flow cytometry was performed as described previously.[31] In brief, mice were injected (i.v.) with 3 μg of BUV395-conjugated anti-CD8α or anti-CD45. After 3 min, mice were sacrificed, and tissues were harvested as described below.

Tissue processing and antibody staining for flow cytometry of lymphocytes

Single cell suspensions were prepared from whole tissues as described previously.[29] In brief, blood was collected into heparinized tubes followed by incubation with RBC lysis buffer. Spleens were mashed through 70-μm strainers, followed by incubation with RBC lysis buffer. For T-cell isolation, brains were chopped into 2-mm pieces before incubation in 1× collagenase D (Sigma-Aldrich) for 1 h, followed by purification using a 40%/60%/90% Percoll (GE Healthcare) gradient.[32] Isolation of brain endothelial cells for flow cytometry was achieved using a previously described method.[7] In brief, brains from mice were minced and shredded with forceps. Tissues were then enzymatically digested in 0.8 mg/mL Dispase II + 0.2 mg/mL Collagenase P + 0.1 mg/mL DNase (all Roche) (4 mL total) in RPMI at 37°C for 15 min with gentle shaking then pipetting up and down every 5 min for an additional 15 min. Following digestion, supernatants were isolated and washed and brain endothelial cell preps were resuspended in a 40% Percoll gradient in HBSS and centrifuged for 10 min at 2000 rpm to remove excess myelin.

After processing, cells were resuspended in FACS buffer and stained for flow cytometry. The following surface markers were used during the preparation of this manuscript: anti-CD8α (BV510, clone 53-6.7), anti-CD31 (PE, clone 390), anti-CD44 (FITC, clone IM7), anti-CD45 (BUV395, clone 30-F11), anti-CD45.1 (BUV737, clone A20), anti-CD45.2 (BV786, clone 104), anti-CD62L (PerCP-Cy5.5, clone MEL-14), anti-CD62P (BUV737, clone RB0.34), anti-EPCR (APC, clone 1560), anti-H-2K^b (BV421, clone AF6-88.5), anti-H-2D^b (PE-Cy7, clone KH95), anti-ICAM1 (BV785, clone YN1/1.7.4), anti-IL-7Rα (PE, clone A7R34), anti-KLRG1 (BV421, clone 2F1), and anti-VCAM1 (FITC, clone 429). Ghost dye 780 (Tonbo Biosciences) was used to measure cell viability and exclude dead cells from analysis. Samples were then fixed using Cytofix fixation buffer (BD Biosciences). For intracellular staining, cells were fixed and permeabilized using Cytofix/Cytoperm buffer (BD Biosciences). Intracellular staining for cytoplasmic proteins was performed for 60 min at 4°C using anti–granzyme B (PE-CF594, clone GB11). All samples were collected using a BD Fortessa flow cytometer.

Immunofluorescence imaging

Immediately following sacrifice, mice were perfused with 30 mL PBS, followed by 15 mL of 1% paraformaldehyde (PFA) in PBS. Brains were carefully removed and placed in 1% PFA overnight at 4°C. Brains were then transferred into a solution containing 30% sucrose for 24 h. Tissues were washed briefly in PBS, lightly blotted to remove excess media, then frozen in Tissue-Tek optimal cutting media (Sakura). Tissue blocks were cut into 20-μm sections using a Leica CM1860 cryostat, then mounted on a slide. Sections were briefly rehydrated using PBS, followed by blocking for 1 h with 5% BSA in PBS. Primary antibody stains were then incubated at 4°C overnight, using the following antibodies: anti-CD31 (AF488, clone MEC13.3), anti-VCAM-1 (AF594, clone 429), and anti-H-2K^b (AF647, clone AF6-88.5). After washing with PBS, a drop of VectaShield Antifade Mounting Medium containing DAPI (Vector Laboratories) was added to each slide, followed by a coverslip.

Fluorescent images were acquired using a Leica Stellaris 8 confocal microscope equipped with an HC PL APO 20× collar-corrected immersion objective (Leica). Spectral positions were set to 430–453 nm (DAPI), 504–556 nm (GFP), 570–610 nm (PE), and 656–710 nm (APC). For analysis of endothelial cell surface markers, 400 μm × 400 μm regions (0.54 μm voxel size) measuring 20 μm thick (1.16 μm voxel size) were captured with a total field of view of $\sim 3.2 \times 10^6$ μm^3. Images were imported into Imaris 10.2 software, and a threshold cutoff was used to reduce CD31 background signal. Surfaces were created around individual blood vessels based on CD31 staining. Surfaces smaller than 1000 μm^3 were excluded from analysis. The mean channel intensity for VCAM-1 and H-2K^b was then measured for individual CD31$^+$ surfaces and normalized to naïve mice.

Thinned-skull window preparation

Thinned-skull windows were prepared as described previously.[33] In brief, mice were anesthetized using a cocktail of ketamine, xylazine, and acepromazine. After a nonresponsive state was demonstrated, the hair over the scalp was removed using clippers. A midline incision was made along the scalp, and a metal bracket was affixed to the skull with glue. A cranial window was then created using an EXL-M40 microdrill (Osada) and microblade (Surgistar), measuring 1.5 mm × 1.5 mm and 20 to 30 μm thick. To visualize blood vessels, 20 μg of Evans blue (MilliporeSigma) dissolved in PBS was injected i.v. 5 min prior to imaging.

Multiphoton microscopy

Following surgery, mice were placed in a custom temperature-controlled chamber attached to the multiphoton microscope. A small pool of artificial cerebrospinal fluid (Harvard Apparatus) was placed above the skull window, and imaging was performed. Mice were imaged using a Leica Stellaris DIVE SP8 multiphoton microscope with an 8000 Hz resonant scanner, an HC IRAPO motCORR 25× water-dipping objective (1.0 NA), an Insight DS laser tuned to 840 nm (for detection of second harmonic signal and GFP), and a Mai Tai DeepSee laser tuned to 930 nm (for detection of Tdtomato [TDT] and Evans blue). A quad HyD non-descanned detector array (4Tune) was used to detect signal with the following spectral positions: 434–492 nm (second harmonic), 512–564 nm (GFP), 580–615 nm (TDT), and 648–700 nm (Evans blue). Line averaging (3) was used to improve the signal-to-noise ratio during image acquisition. For each animal, between 1 and 3 unique positions were captured, each measuring ∼350 μm × ∼350 μm (0.693 μm voxel size) with z stacks ranging between 60 μm and 120 μm (3 μm voxel size). Imaging sessions lasted for 45 to 90 min, with ∼30-s capture intervals.

Following image acquisition, all files were spectrally unmixed using LAS X software (Leica), then imported into Imaris 10.2 (Bitplane). After correcting for drift from any movement artifacts, a Gaussian filter (width corresponding to pixel size) was applied to each movie to lessen noise and smooth the image. Tracks were created using the spots function for GFP^+ and TDT^+ events with the following parameters: 10 μm spot size, 3 frames maximum gap size, 20 μm maximum distance between spots, and 5 min minimum track duration. Tracks were manually corrected where necessary, and statistics were exported for downstream analysis.

Data analysis

All flow cytometry data were analyzed using FlowJo software (v10.10). For multiphoton analysis, the mean velocity (track speed mean) and arrest coefficient (proportion of time that a cell was arrested <4 μm/min) were calculated for all GFP^+ and TDT^+ tracks. For analysis of confocal images, the mean channel intensity for each marker of interest was measured based on $CD31^+$ surfaces. In main figures, confocal data are normalized to the average expression in naïve mice. All graphs were created in GraphPad Prism 10 and figures were assembled in Adobe Illustrator version 30.8.1.

Statistical analysis

All data analysis was performed using GraphPad Prism 10. Data were evaluated for statistical significance using a Mann–Whitney test for comparison of 2 groups, or Kruskal–Wallis test followed by Dunn's test for 3 or more groups unless stated otherwise. To compare independent intravital imaging experiments, random sampling was used to select 50 individual OT-I T-cell tracks from each animal, and migration parameters were compared on a per-experiment basis using a Mann–Whitney U test. Unless otherwise stated, *n* represents the number of animals used in an experiment and is stated in the legend for each figure. A *P* value <0.05 was considered statistically significant.

Results

Treatment with IL-15C expands CD8 T cells but does not change migration to the cerebral vasculature

In this study we utilized transgenic OT-I T cells, which recognize OVA peptide. These cells respond similarly to *Plasmodium*-specific GAP50 tetramer-positive endogenous cells[29] and enable the use of fluorescent reporters, which were integral for this work. Naïve OT-I T cells ($CD45.1^+$) were transferred into C57BL/6 mice, followed by infection with PbA expressing mCherry-OVA (PbA-OVA).[28] On days 2 and 3 p.i., mice were treated with IL-15C to reduce the incidence of ECM.[17] Consistent with our previous work,[17] parasitemia levels in the blood were not affected by IL-15C treatment (Fig. S1A). On day 7 p.i. when untreated mice became symptomatic, tissues were collected and prepared for flow cytometry (Fig. 1A–C and Fig. S1B). Endogenous cells ($CD44^+CD45.1^-$) and transgenic OT-I T cells ($CD44^+CD45.1^+$) were compared between untreated and IL-15C–treated mice.

We found that IL-15C treatment significantly reduced the frequency of OT-I T cells in the spleen and blood (Fig. 1D). However, the number of OT-I T cells in the blood was increased by IL-15C treatment (Fig. 1E), and we found a similar trend in OT-I numbers in the spleen. Because the frequency of OT-I T cells was reduced while the quantity of cells was increased, these data suggest that IL-15 stimulation induces proliferation among both the endogenous and transferred CD8 T-cell pools. As expected, endogenous CD8 T cells in the spleen and blood expanded significantly following IL-15C treatment (Fig. S1C). In the brain, both the frequency and number of OT-I T cells was unaffected by IL-15C treatment, consistent with our earlier findings.[17]

We next used intravascular labeling[31] to ask whether IL-15C changes the localization of OT-I T cells within the spleen and brain (Fig. S1D). IL-15C treatment decreased the frequency of intravascular-positive (IV^+) cells among both the endogenous and OT-I T cells in the splenic red pulp, with more OT-I T cells found in the intravascular-negative (IV^-) white pulp (Fig. 1F, G and Fig. S1E). In the brain, there was no change in the localization of OT-I T cells, with most cells from both groups being found in the IV^+ fraction, demonstrating their presence in the cerebral vasculature (Fig. 1H, I and Fig. S1E).

As expected from our previous work, we found an increase in the number of NK cells after IL-15C treatment across all analyzed tissues (Fig. S1F). We also characterized the localization of NK cells using intravascular labeling during PbA infection. In the spleen, most NK cells were localized to the white pulp in untreated mice. IL-15C increased the frequency of IV^+ staining (Fig. S1G), in contrast to CD8 T cells (Fig. 1F and Fig. S1E), suggesting that in IL-15C–treated mice more NK cells are entering circulation. In the brain, most NK cells were

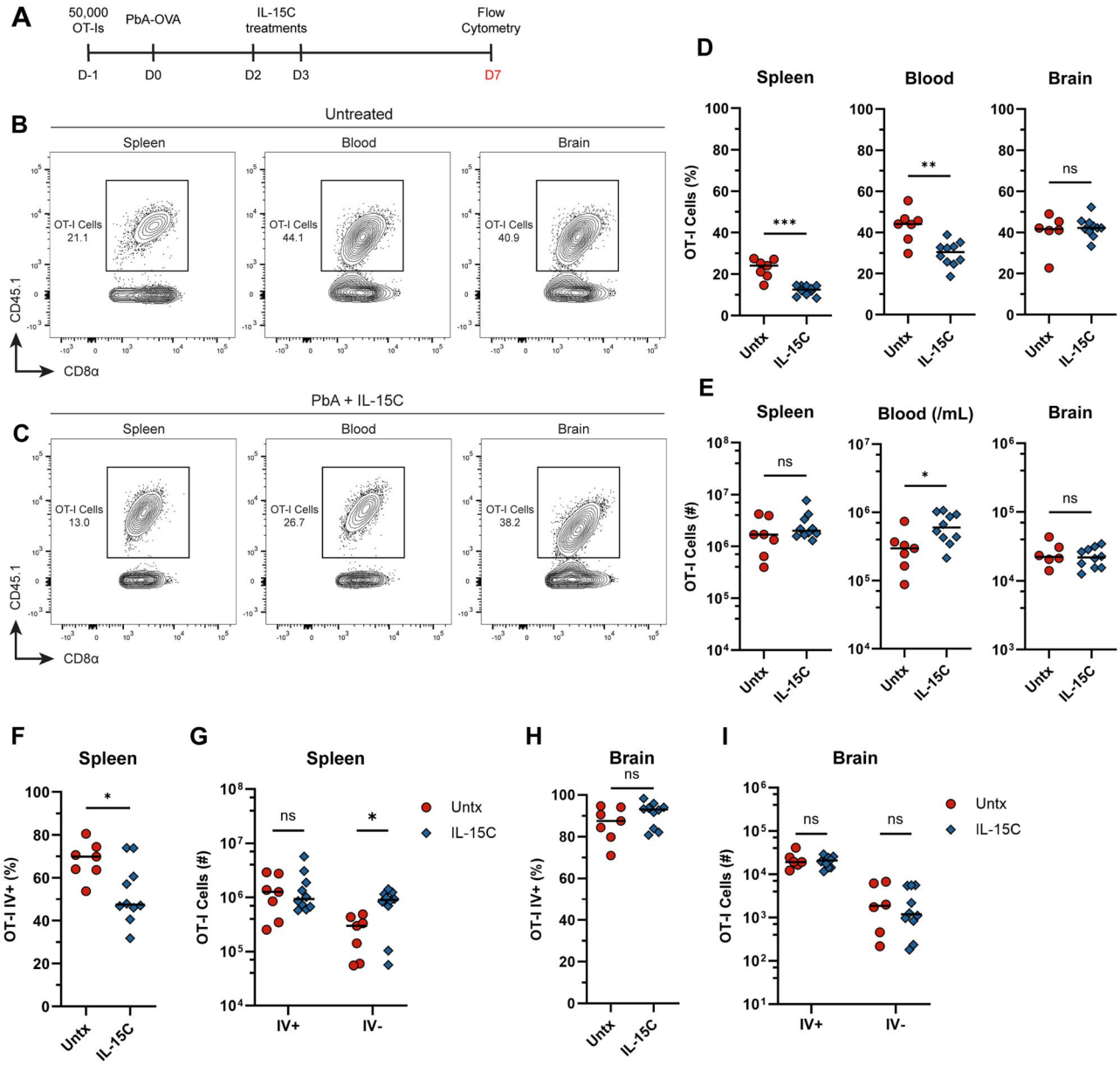


Figure 1 Treatment with IL-15C expands CD8 T cells but does not alter their migration to the cerebral vasculature during PbA infection. (A) Experimental schematic for Figs. 1 and 2: Mice were seeded with 5×10^4 CD45.1$^+$ OT-I T cells before infection with PbA-OVA. On days 2 and 3 postinfection (p.i.), some mice received treatment with IL-15C. On day 7 p.i., tissues were collected and prepared for flow cytometry. (B, C) Representative flow cytometry plots of CD45.1$^+$ OT-I T cells in the spleen, blood, and brain on day 7 p.i. with PbA-OVA, in either untreated (B) or IL-15C–treated (C) mice. (D) Frequency of CD45.1$^+$ OT-I T cells in the indicated tissues on day 7 p.i. with PbA-OVA in either untreated (red) or IL-15C–treated (blue) mice. Values represent the frequency of CD45.1$^+$ cells among the responding (CD44$^+$) effector T-cell pool. (E) Total number of CD45.1$^+$ OT-I T cells in the indicated tissues on day 7 p.i. with PbA-OVA in either untreated or IL-15C–treated mice. (F) Frequency of intravascular (IV) label-positive OT-I T cells in the spleen on day 7 p.i. with PbA-OVA in either untreated or IL-15C–treated mice. (G) Total number of IV$^+$ or IV$^-$ OT-I T cells in the spleen on day 7 p.i. with PbA-OVA in either untreated or IL-15C–treated mice. (H) Frequency of IV label-positive OT-I T cells in the brain on day 7 p.i. with PbA-OVA in either untreated or IL-15C–treated mice. (I) Total number of IV$^+$ or IV$^-$ OT-I T cells in the brain on day 7 p.i. with PbA-OVA in either untreated or IL-15C–treated mice. Plots in (B, C) are representative of 3 independent experiments. Data in (D–I) are combined from 3 independent experiments with $n = 2$–5 mice per group and analyzed with a Mann–Whitney U test, with the horizontal line representing the median. $^*P < 0.05$, $^{**}P < 0.01$, $^{***}P < 0.001$. See also Fig. S1. ns, not significant; Untx, untreated.

found in the vasculature, and this was not altered by IL-15C treatment. Collectively, these data show that while IL-15C treatment induces moderate differences in CD8 T cells and NK cell number and location within the spleen and blood, their migration to and localization within the brain are largely unaffected.

IL-15C treatment reduces granzyme B expression but does not improve the formation of memory precursor effector cells

Since OT-I T cells still migrate to the brain in IL-15C–treated mice, but do not cause lethal immunopathology, we hypothesized that T cells may express lower levels of effector molecules following treatment. Granzyme B expression by CD8 T cells is required for the development of ECM in mice[12] and is highly expressed in human brains of those who die from CM.[13] On day 7 p.i., tissues were collected from untreated mice and those receiving IL-15C and stained for granzyme B directly ex vivo.

In the spleen, granzyme B expression was low for both endogenous CD8 T cells and transgenic OT-I T cells (Fig. S2A, C). However, in the blood, its expression was common, and IL-15C treatment reduced the proportion of both endogenous and transgenic CD8 T cells expressing this effector molecule (Fig. 2A and Fig. S2B, C). The geometric fluorescence intensity of granzyme B was also reduced in the blood of IL-15C–treated mice, though this did not reach significance (Fig. 2B, C). Surprisingly, neither the frequency nor number of granzyme B–expressing OT-I T cells in the brain was changed with IL-15C treatment (Fig. 2D and Fig. S2B). However, expression was reduced on a per-cell basis, with a lower geometric mean fluorescence intensity (gMFI) in treated mice (Fig. 2E, F). Among endogenous CD8 T cells, we found a reduction in the frequency of granzyme B–expressing cells in the brain (Fig. S2C). Collectively, these data show that IL-15C treatment restricts CD8 T-cell expression of effector molecules in the brain, which may reduce ECM-related immunopathology.[12]

Effector CD8 T cells can be grouped into 2 different subsets, either KLRG1$^+$ short-lived effector cells (SLECs) or IL-7Rα^+ memory precursor effector cells (MPECs). The ratio of MPECs to SLECs is influenced by the inflammatory milieu present during priming, with high inflammation leading to a more SLEC-biased pool of effector CD8 T cells.[34] We recently reported that PbA infection induces a unique pattern of differentiation among responding CD8 T cells, with a strong bias toward SLECs and very few MPECs.[29] Given the immunosuppressive effects of IL-10, we hypothesized that the increased production of IL-10 by IL-15C–stimulated NK cells might amplify the proportion of MPECs during the effector phase. We found more MPECs in the spleen of untreated mice than other tissues, but this was still a very minor population compared to SLECs (Fig. 2G–I and Fig. S2D–F). Contrary to our hypothesis, IL-15C did not improve the formation of MPECs in any tissue and led to more SLECs in the blood (Fig. S2E), with a corresponding reduction in the MPEC:SLEC ratio (Fig. 2I). Taken together, these data indicate that IL-15C modulates granzyme B expression by CD8 T cells during PbA infection but does not alter CD8 T-cell effector differentiation.

IL-15C reduces CD8 T-cell arrest in the brains of malaria-infected mice

While flow cytometry can survey the phenotype and localization of cells at one specific time point during the immune response, it does not capture the behavior of immune cells in real time. During ECM pathogenesis, CD8 T cells arrest along the vasculature of the brain and cause lethal immunopathology. Given that cerebral disease is prevented by administration of IL-15C, we hypothesized that the OT-I T cells in IL-15C–treated mice would be less prone to arrest along the vascular endothelium, coinciding with a faster track velocity. To test this, we used intravital microscopy to study interactions between CD8 T cells and the vascular endothelium of the brain.

On the day prior to infection, OT-I T cells expressing GFP were transferred into VE-cadherin^{CreERT2} mice expressing Tdtomato (VE-cadherin TDT) that were recently treated with tamoxifen. These mice were then infected with PbA-OVA, followed by treatment with IL-15C (Fig. S3A). On day 6 to 7 p.i., when mice started to develop symptoms of ECM, mice were anesthetized and thinned-skull windows were prepared (Fig. S3B) as described previously.[33] Prior to imaging, mice were injected with Evans blue to visualize blood vessels and placed in a temperature-controlled chamber to perform multiphoton microscopy.

In both groups of mice, individual OT-I T cells displayed highly variable migration dynamics (Fig. 3A, B and Videos S1, S2). We created tracks for individual OT-I T cells from each representative video and assessed their movement in vivo (Fig. S3C, D). In untreated mice, OT-I T cells were migrating at a significantly slower rate as compared to mice receiving IL-15C treatment (Fig. 3C). This corresponded with an elevated arrest coefficient (percent time moving $<4\,\mu$m/min) in untreated mice (Fig. 3D). While capturing videos in untreated mice, we occasionally observed small areas that contained many arresting OT-I T cells (Video S3), while other vessels in the same field of view contained few OT-I T cells. These data are consistent with studies of cerebral immunopathology in other model systems that have highlighted the heterogeneity of microvessels in the brain,[35] with postcapillary venules being an “activity hotspot” of CD8 T-cell clustering during PbA infection.[36]

OT-I T-cell movement dynamics across experiments

While we found that IL-15C treatment induces significant changes in OT-I T-cell movement, we wanted to evaluate how reproducible these effects were when compared across different mice analyzed in 4 independent experiments. We took a random sample of 50 OT-I T-cell tracks from each animal to account for numerical differences in the quantity of OT-I T cells between timelapses. The mean velocity and arrest coefficient were then plotted, comparing untreated and IL-15C–treated mice from the same imaging session. We found that OT-I T-cell velocity in IL-15C–treated mice was increased in 4 representative experiments, but only reached significance in 2 of 4 experiments (Fig. 3C, D and Fig. S4A–C). Increased velocity also coincided with a decreased arrest coefficient in 3 of 4 experiments.

In all imaging sessions, OT-I T cells demonstrated variable movement characteristics, with dynamic changes in velocity over the course of each timelapse. Even in mice with noticeable ECM symptoms, some OT-I T cells were observed moving at velocities $>15\,\mu$m/min. We wanted to focus specifically on the slow moving or arrested cells that cause immunopathology. In doing so, we found that untreated mice had a greater number of tracks per video with a mean velocity of $<4\,\mu$m/min than IL-15C–treated mice (Fig. 3E). Similarly, the number of tracks per video with an

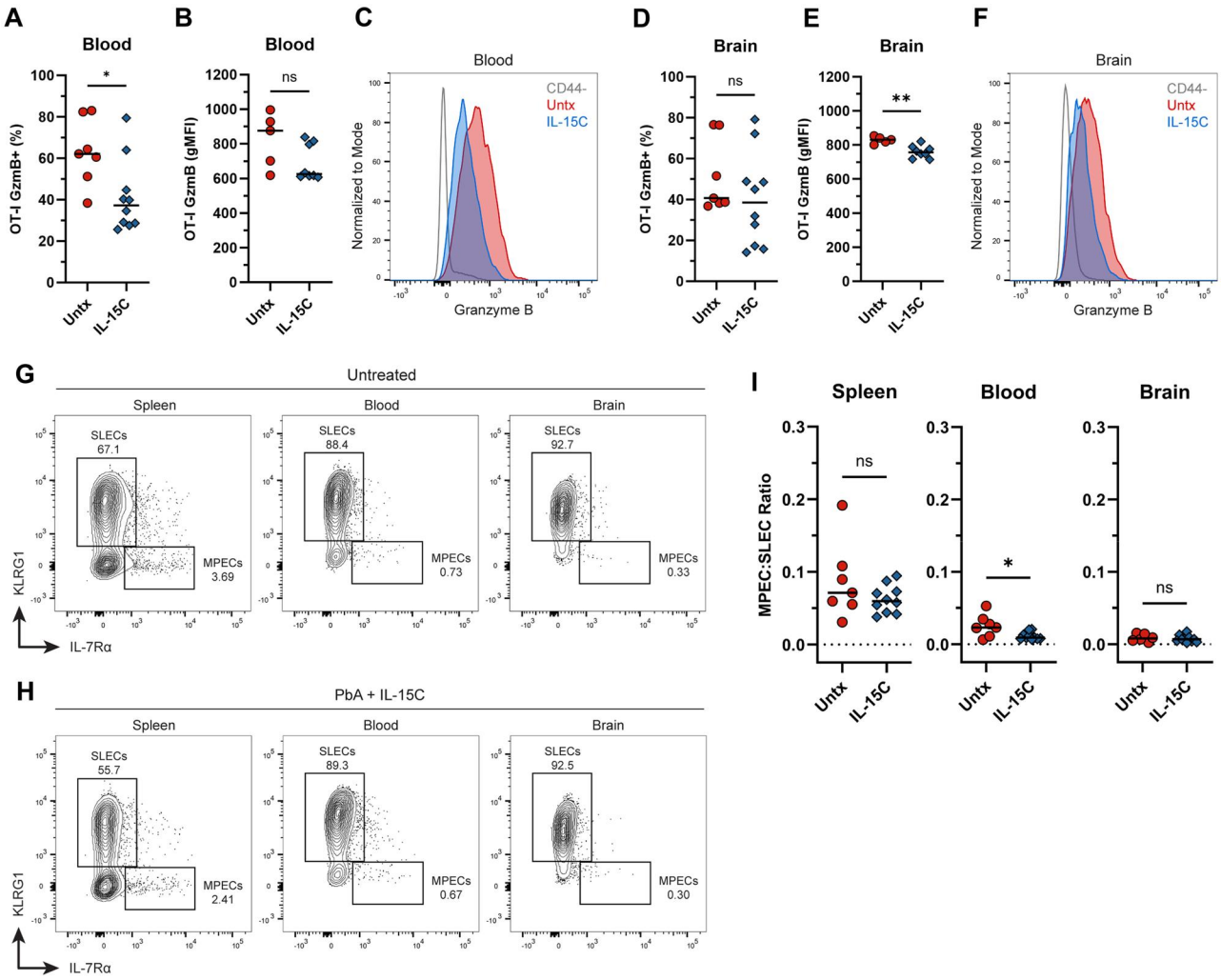


Figure 2 IL-15C treatment reduces granzyme B (GzmB) expression but does not improve the formation of memory precursor effector cells. (A) Frequency of OT-I T cells in the blood expressing GzmB directly ex vivo on day 7 p.i. with PbA-OVA from either untreated (red) or IL-15C–treated (blue) mice. (B) Geometric mean fluorescence intensity (gMFI) of GzmB after gating on GzmB$^+$ OT-I T cells in the blood from either untreated or IL-15C–treated mice on day 7 p.i. with PbA-OVA. (C) Representative histograms of GzmB expression by either CD44$^-$ cells (gray), or OT-I T cells from untreated (red) or IL 15C–treated (blue) mice in the blood on day 7 p.i. with PbA-OVA. (D) Frequency of OT-I T cells in the brain expressing GzmB directly ex vivo on day 7 p.i. with PbA-OVA from either untreated or IL-15C–treated mice. (E) gMFI of GzmB after gating on GzmB$^+$ OT-I T cells in the brain from either untreated or IL-15C–treated mice on day 7 p.i. with PbA-OVA. (F) Representative histograms of GzmB expression by either CD44$^-$ cells, or OT-I T cells from untreated or IL 15C–treated mice in the brain on day 7 p.i. with PbA-OVA. (G, H) Representative KLRG1 × IL-7Rα flow cytometry plots showing the effector phenotype of OT-I T cells in the indicated tissues on day 7 p.i. with PbA-OVA in either untreated (C) or IL-15C–treated (D) mice. (I) Ratio of IL-7Rα^{hi} KLRG1$^-$ memory precursor effector cell (MPEC) phenotype to IL-7Rα^{lo} KLRG1$^+$ short-lived effector cell (SLEC) phenotype after gating on CD45.1$^+$ OT-I T cells in the indicated tissues on day 7 p.i. with or PbA-OVA. Plots in (C, F–H) are representative of 3 independent experiments. Data in (A, B, D, E, I) are combined from 3 independent experiments with $n = 2$–5 mice per group and analyzed with a Mann–Whitney U test, with the horizontal line representing the median. *$P < 0.05$, **$P < 0.01$. See also Fig. S2. ns, not significant; Untx, untreated.

arrest coefficient of >0.8 is reduced by IL-15C treatment (Fig. 3F), indicating that fewer highly arrested CD8 T cells are present in treated mice. We also found a decrease in the total number of OT-I tracks in IL-15C–treated mice (Fig. S4D).

Prior to thinned-skull window surgery and imaging, we scored mice based on ECM symptoms, to prevent variance in disease severity from confounding our analysis. We report a positive correlation between the number of slow-moving tracks and disease severity (Fig. S4E, F). This is consistent with previous work demonstrating the relationship between arresting CD8 T cells and development of ECM.[7] Altogether, our data indicate that IL-15C treatment reduces the number of arresting CD8 T cells in the brain, which rescues mice from lethal disease.

Intravital imaging of NK cells in the mouse brain during cerebral malaria

After finding that CD8 T-cell arrest is mitigated by IL-15C treatment, we asked whether CD8 T cells and NK cells were frequently making direct contact within the cerebral vasculature.

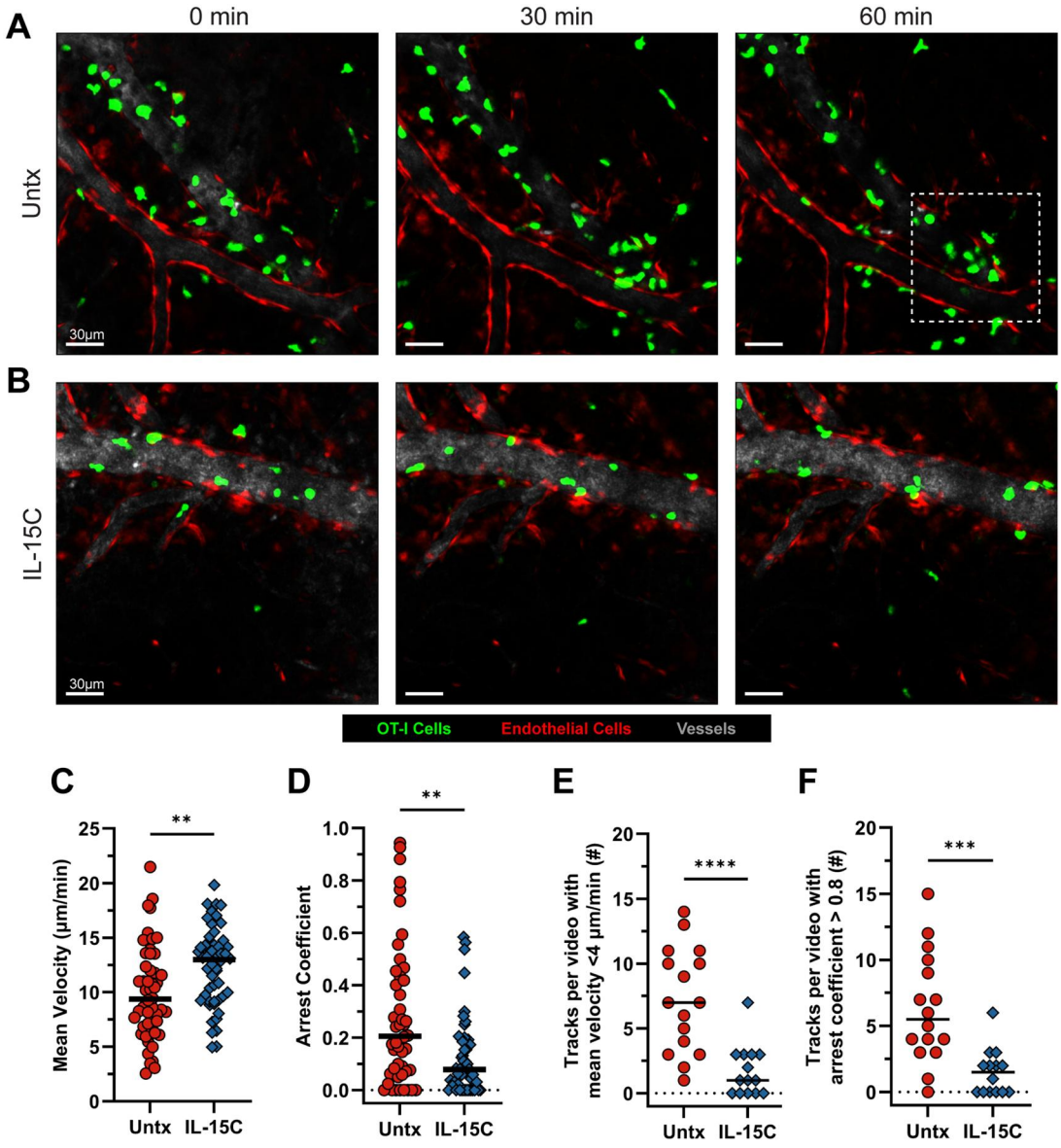


Figure 3 IL-15C reduces CD8 T-cell arrest in the brains of *Plasmodium berghei*-infected mice. (A, B) Representative maximal projections of 3D timelapses captured through a thinned-skull window of either untreated (A) or IL-15C–treated (B) mice. TDT$^+$ endothelial cells are shown in red, OT-I GFP$^+$ T cells are shown in green, and blood flow is visualized using Evans blue (gray). Time points are denoted as minutes. Scale bars represent 30 μm. See corresponding Videos S1 and S2. White box represents an area of significant OT-I T-cell arrest; see Video S3 (stars indicating arrested cells). (C, D) Quantification of cell velocities (C) and arrest coefficients (D) from 50 randomly sampled OT-I T-cell tracks on day 7 p.i. from the mice in the representative experiments from Videos S1 and S2, which were either untreated (red) or IL-15C treated (blue). Each dot represents an individual T-cell track, and horizontal black lines denote the group median. (E, F) Total number of tracks per 3D timelapse with a mean velocity of <4 μm/min (E) or an arrest coefficient >0.8 (F), from either untreated or IL-15C–treated mice. Each dot represents the number of tracks with the specified characteristics from one timelapse. Images in (A, B) are representative projections of 4 independent experiments as shown in Videos S1 and S2. Data in (C, D) are compared from the first experiment, shown in Videos S1 and S2. Data in (E, F) are combined from 6 untreated mice (16 unique positions) and 5 IL-15C–treated mice (14 unique positions) across 6 independent experiments. Data in (C–F) were analyzed with a Mann–Whitney U test, with the horizontal line representing the median. $^{**}P < 0.01$, $^{***}P < 0.001$ $^{****}P < 0.0001$. See also Figs. S3 and S4. Untx, untreated.

NK cells have not been imaged in the brain during PbA infection, so the speed and behavior of this population is unknown. Ncr1^{iCre} mice were crossed to Ai14 mice, specifically expressing TDT in NK cells. Mice were prepared as above, and intravital imaging was performed (Fig. 4A, B and Videos S4, S5).

We quantified NK cell movement dynamics in the presence or absence of IL-15C. We found that, similar to OT-I T cells, IL-15C treatment led to a higher overall mean track velocity and lower arrest coefficient compared to untreated mice (Fig. 4C, D). These studies also revealed a trending increase in the number of NK cell tracks in the brain of IL-15C–treated mice as compared to untreated mice (Fig. 4E). Of note, across multiple animals in either group, we did not observe any sustained interactions between OT-I T cells and NK cells. Our data indicate that if direct

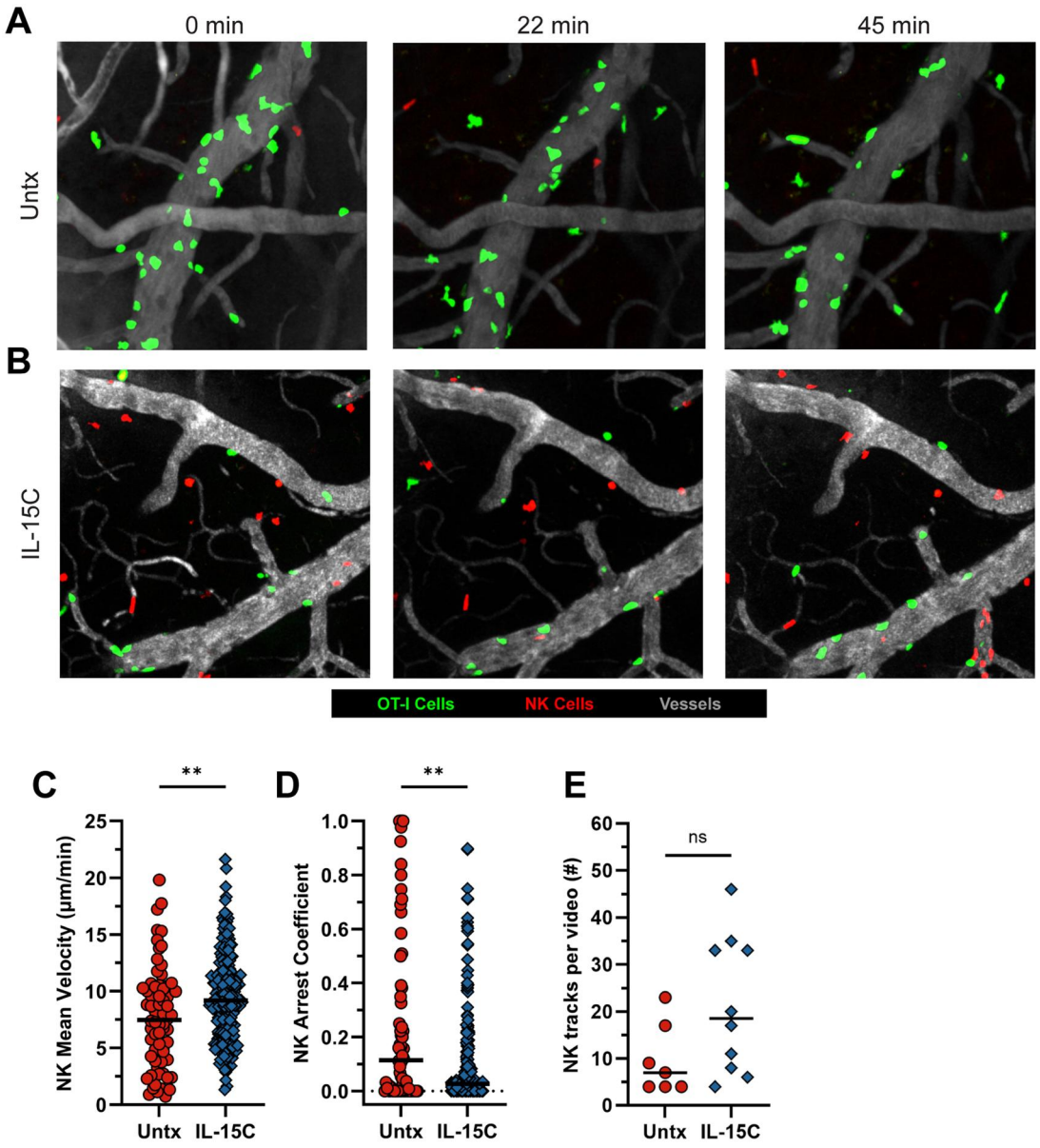


Figure 4 Intravital imaging of NK cells in the mouse brain during cerebral malaria. (A, B) Representative maximal projections of 3D timelapses captured through a thinned-skull window of either untreated (A) or IL-15C–treated (B) mice. NK^{iCre} TDT (red) mice were seeded with 5×10^4 OT-I GFP^+ T cells (green) on the day prior to infection with PbA-OVA. Blood flow was visualized using Evans blue (gray), injected 5 min prior to imaging. Time points are denoted as minutes. Scale bars represent 30 μm. See corresponding Videos S4 and S5. (C) The total number of NK cell tracks per field of view is represented, comparing untreated mice (red) with IL-15C–treated mice (blue). (D, E) Quantification of NK cell velocities (C) and arrest coefficients (D) from all mice combined from 4 independent experiments, which were either untreated (red) or IL-15C treated (blue). Each dot represents an individual NK cell track, and horizontal black bars denote the group median. Images in (A, B) are representative projections of 4 independent experiments. Data in (C–E) are combined from 4 untreated mice (7 unique positions) and 5 IL-15C–treated mice (10 unique positions) across 4 independent experiments with $n = 1$–2 mice per group. Data in (C–E) were analyzed with a Mann–Whitney U test, with the horizontal line representing the median. $^{**}P < 0.01$. ns, not significant; Untx, untreated.

regulation is occurring between IL-10–secreting NK cells and OT-I T cells, these interactions are either happening elsewhere, or they do not require sustained contact in the brain. Additionally, similar to our findings with OT-I T cells, IL-15C treatment increased NK cell velocity and reduced arrest. These results suggest that CD8 T cells and NK cells may use similar migration programs to move through the brain during PbA infection.

CD8 T-cell expression of IL-10Rα is not required for IL-15C–mediated prevention of cerebral malaria

Next, we wanted to determine which cells were being modulated by the NK cell–secreted IL-10 induced by IL-15C. This regulation could either occur directly, through CD8 T-cell sensing of

IL-10, or it could occur indirectly by modifying antigen presentation or adhesion molecule expression by endothelial cells. To this end, we tested whether deletion of IL-10Rα on CD8 T cells would abrogate the protective effect of IL-15C treatment. We validated the deletion of IL-10Rα specifically on CD8 T cells in IL-10Rα$^{fl/fl}$ mice crossed to E8i-Cre (CD8^{Cre}) using rtPCR (Fig. S5A). CD8^{Cre} × IL-10Rα$^{fl/fl}$ mice were then infected with PbA, followed by treatment with IL-15C, and then mice were monitored for the development of ECM (Fig. S5B). Most CD8^{Cre-} and CD8^{Cre+} mice succumbed to ECM on day 6 to 8 p.i. without IL-15C treatment (Fig. S5C). Surprisingly, we found that all IL-15C–treated mice were protected from ECM, even in animals whose CD8 T cells could not sense IL-10. This was not due to differences in parasite burden, as parasitemia levels were similar between groups (Fig. S5D). We also validated these findings using flow cytometry by gating on endogenous CD44$^+$ CD8 T cells. As before, there were no differences in the number of CD44$^+$ CD8 T cells in the blood or brain across all 4 groups (Fig. S5E). There was also no change in the proportion of granzyme B–expressing endogenous CD8 T cells when comparing IL-15C–treated CD8^{Cre-} and CD8^{Cre+} mice (Fig. S5F), consistent with improved survival regardless of IL-10R expression by CD8 T cells. These data show that CD8 T-cell expression of IL-10Rα is dispensable for the prevention of ECM by IL-15C treatment.

IL-15C treatment reduces endothelial cell expression of adhesion and MHC-I molecules in the brain

During malaria infection, vascular endothelial cells in the brain upregulate cellular adhesion molecules and cross-present malaria antigen, which are associated with T-cell arrest during ECM.[6,7,37,38] Given that both T cells and NK cells were less prone to arrest following IL-15C treatment, we hypothesized that IL-15C could be reducing endothelial cell expression of adhesion molecules during ECM. We also hypothesized that MHC-I levels would be reduced by IL-15C treatment, since IL-10 has been shown to regulate its expression on endothelial cells.[39,40] To investigate this, we isolated brain endothelial cells for flow cytometry and stained for various markers that are associated with ECM (Fig. 5A and Fig. S6A). We found that IL-15C reduced both the proportion of VCAM-1$^+$ cells and the overall expression as measured by gMFI (Fig. 5B). Interestingly, nearly all brain endothelial cells expressed ICAM-1 and H-2K^b during PbA infection (Fig. 5C, D). However, the gMFI for both surface receptors was reduced with IL-15C treatment. H-2D^b expression was only expressed by approximately half of brain endothelial cells but was also reduced by IL-15C treatment (Fig. 5E). Endothelial cell protein C receptor (EPCR) and P-selectin (CD62P) can enhance sequestration of infected RBCs to the vessel endothelium and have been implicated in severe malaria of both mice and humans.[41–46] We report that the expression of both surface receptors was reduced when mice are treated with IL-15C (Fig. S6B, C).

We also sectioned brains from PbA-infected mice with or without IL-15C treatment on day 7 p.i., using anti-CD31 antibody to identify endothelial cells via confocal microscopy (Fig. S7A–C). Naïve mice expressed relatively low levels of VCAM-1 and H-2K^b. In line with our flow cytometry data, infected mice upregulated VCAM-1, and IL-15C treatment reduced expression on CD31$^+$ vessels (Fig. S7D). However, although reduced, VCAM-1 expression was still elevated in IL-15C–treated mice as compared to uninfected mice. As measured by confocal microscopy, there was no difference in H-2K^b expression on endothelial cells between untreated and IL-15C–treated mice at this time point (Fig. S7E), although a small proportion of vessels in untreated mice expressed high levels of H-2K^b that was otherwise absent in mice receiving IL-15C treatment. Overall, these results show that IL-15C modulates the expression of key surface receptors involved in CD8 T-cell engagement with the endothelium. This in turn leads to fewer CD8 T cells arresting along the vascular endothelium and protects mice from blood-brain barrier disruption and ECM development.

Endothelial cell expression of IL-10Rα is necessary for prevention of cerebral malaria

Since brain endothelial cells can also express IL-10Rα,[47] we considered whether NK cell–secreted IL-10 could be directly modulating endothelial cells in the brains of IL-15C–treated mice. We generated mice with conditional deletion of IL-10Rα on endothelial cells (VE-cadherin^{CreERT2} TDT × IL-10Rα$^{fl/fl}$). These mice were then infected with PbA, and some groups received treatment with IL-15C. As before, parasitemia was measured prior to symptom onset to ensure that parasite burden was equal between groups (Fig. S7F). As expected, IL-15C treatment was protective in mice whose endothelial cells could sense IL-10. However, this effect was significantly reduced in mice lacking endothelial cell expression of IL-10Rα (Fig. 5F).

We then asked if loss of IL-10Rα expression on endothelial cells is required for the downregulation of adhesion molecules and MHC-I, which we observed in WT mice (Fig. 5A–E). To test this, we isolated brain endothelial cells for flow cytometry from VE-cadherin^{CreERT2} TDT × IL-10Rα$^{fl/fl}$ mice following PbA infection (Fig. 5A). We first validated Cre-recombinase activity in CD31$^+$ cells by quantifying expression of TDT in tamoxifen-treated mice. Following tamoxifen treatment, approximately 80% of CD31$^+$ endothelial cells expressed TDT (Fig. S7G). TDT expression was occasionally observed in mice without tamoxifen treatment, suggesting variable low to moderate Cre activity in some untreated animals. However, we found little to no expression of TDT in CD45$^+$ cells in either tamoxifen- or vehicle-treated mice, confirming the endothelial cell specificity of the Cre activity (Fig. S7G). When endothelial cells lacked IL-10Rα, IL-15C treatment did not reduce expression of VCAM or H-2K^b (Fig. 5G, H). Thus, rather than NK cell–secreted IL-10 acting directly upon CD8 T cells during ECM, these data support that IL-15C treatment protects mice from ECM by modulating vascular endothelial cell activation, and that this is dependent upon endothelial cell expression of IL-10Rα.

Discussion

Cerebral malaria is a devastating complication of *Plasmodium* infection that remains poorly understood. In the clinic, children

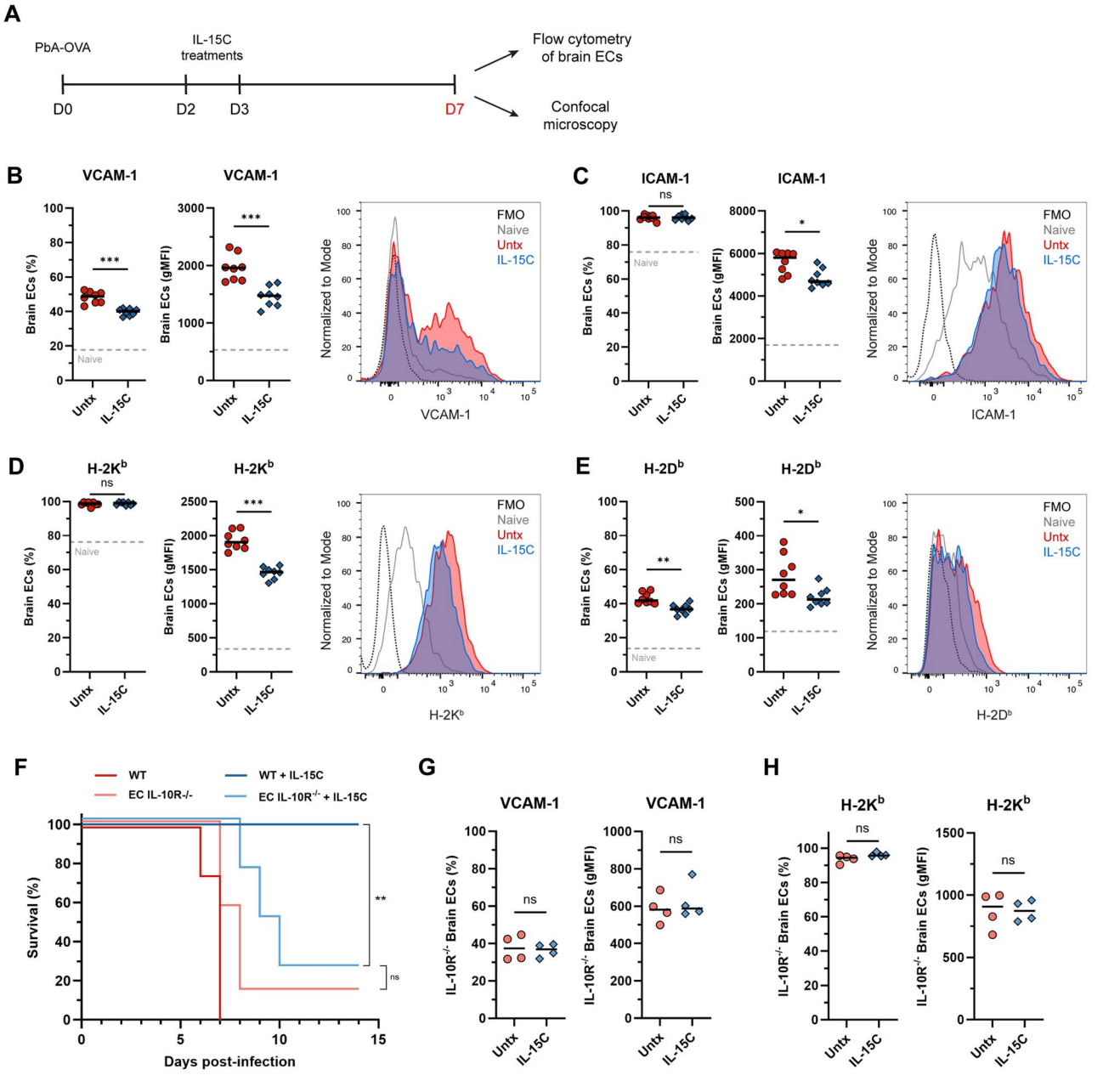


Figure 5 IL-15C treatment reduces antigen presentation and adhesion molecule expression by endothelial cells in the brains of malaria-infected mice. (A) Experimental schematic for Fig. 5. Mice were infected with PbA-OVA, followed by treatment with IL-15C on days 2 and 3 p.i. On day 7 p.i., brains were collected from mice and were either frozen for tissue sectioning or prepared for flow cytometry of brain endothelial cells (ECs) . (B) Staining frequency (left), gMFI (middle), and representative histograms for VCAM-1 expression by brain ECs in either untreated (red) or IL-15C–treated (blue) mice. Naïve expression is represented by the gray line, and fluorescence-minus-one (FMO) controls are shown in black. (C) Staining frequency (left), gMFI (middle), and representative histograms (right) for ICAM-1 expression by brain ECs in either untreated or IL-15C–treated mice. Naïve expression is represented by the gray line, and FMO controls are shown in black. (D) Staining frequency (left), gMFI (middle), and representative histograms (right) for H-2K^b expression by brain ECs in either untreated or IL-15C–treated mice. Naïve expression is represented by the gray line, and FMO controls are shown in black. (E) Staining frequency (left), gMFI (middle), and representative histograms (right) for H-2D^b expression by brain ECs in either untreated or IL-15C–treated mice. Naïve expression is represented by the gray line, and FMO controls are shown in black. (F) Survival curve showing VE-cadherin^{Cre-} × IL-10Rα$^{fl/fl}$ mice and VE-cadherin^{Cre+} × IL-10Rα$^{fl/fl}$ mice that were either untreated (red) or treated with IL-15C (blue). (G) Staining frequency (left) and gMFI (right) of VCAM-1 on brain ECs from VE-cadherin^{Cre+} × IL-10Rα$^{fl/fl}$ mice that were either untreated (light red) or treated with IL-15C (light blue) on day 7 p.i., with PbA-OVA. (H) Staining frequency (left) and gMFI (right) of H-2K^b on brain ECs from VE-cadherin^{Cre+} × IL-10Rα$^{fl/fl}$ mice that were either untreated (light red) or treated with IL-15C (light blue) on day 7 p.i. with PbA-OVA. Data in (B–E) are combined from 2 independent experiments with $n = 4$ mice per group and analyzed with a Mann–Whitney U test. Data in (F) are representative of 3 independent experiments with the following groups: WT ($n = 8$), WT + IL-15C ($n = 8$), EC IL-10R$^{-/-}$ ($n = 7$), or EC IL-10R$^{-/-}$ + IL-15C ($n = 8$), analyzed with a log-rank Mantel–Cox test. Data in (G, H) are representative of 2 independent experiments with a total of $n = 4$ mice per group. Horizontal lines represent the group median. *$P < 0.05$, **$P < 0.01$, ***$P < 0.001$. See also Figs. S6 and S7. ns, not significant; Untx, untreated.

with CM are given antimalarial drugs and other supportive care, but no therapies that specifically inhibit the hyperinflammatory immune response have been approved for treatment.[48] We previously reported that treatment with IL-15C rescues mice from developing ECM, and that this phenomenon was dependent on IL-10 secretion by NK cells. In this study, we scrutinized the mechanism by which IL-15C prevents the development of cerebral pathology in mice. Using flow cytometry, we found that IL-15C had little impact on the number of CD8 T cells found in the brain during ECM development. CD8 T-cell expression of granzyme B is necessary for mice to develop ECM, and our data show that treatment with IL-15C reduces its expression by CD8 T cells in the cerebral vasculature of PbA-infected mice. CD8 T cells also accumulate in the brain during human CM, and these cells express high levels of granzyme B.[13] While our data are gathered from an experimental malaria model in mice, our results suggest that IL-15C treatment could be a promising immunotherapy to prevent CM in humans, especially considering that similar IL-15 complexes have been used in clinical trials for HIV and solid tumors.[49–51] Alternative treatments that also reduce CD8 T-cell arrest during CM, such as adhesion molecule blockade, could be promising therapeutics to prevent disease. Such inhibitors have been used in other clinical settings of autoimmunity with varying degrees of success,[52–54] but no trials have been conducted in CM.

We employed thinned-skull window surgeries together with multiphoton microscopy to study interactions between CD8 T cells and the vascular endothelium in the brain. In untreated mice, we observed significant regions of OT-I T-cell arrest in the cerebral vasculature. Of note, these areas were not present in all cerebral vessels but were typically limited to one or 2 regions in each field of view, with other vessels showing very little arrest. These observations support a model in which certain "activity hotspots" may account for the majority of T-cell arrest and immunopathology.[36] We found that IL-15C treatment reduces the number of arresting T cells within the brain, corresponding with a higher track velocity. When we focused specifically on arrested cells, there were more slow-moving or arrested CD8 T cells in untreated mice than those receiving IL-15C. CD8 T-cell arrest is directly associated with ECM development, as both genetic knockout and antibody-mediated blockade of cellular adhesion molecules prevents T-cell arrest and promotes survival.[7,55] Our work substantiates these data, again indicating that therapies which reduce T-cell arrest could prevent disease or lessen severity. We also measured NK cell movement dynamics in the brain and asked if these were affected by treatment. Interestingly, NK cell movement was affected similarly to CD8 T cells, with IL-15C treatment leading to less overall NK cell arrest within the brain. These results suggest that NK cells and CD8 T cells use similar migration processes during ECM.

Next, we explored the target cell for NK cell–secreted IL-10 that is being modulated in response to IL-15C treatment. We tested if IL-10 from NK cells would act directly upon CD8 T cells by decreasing their effector function. However, we made the surprising observation that when IL-10Rα was removed from CD8 T cells, IL-15C still protected mice from ECM, suggesting an indirect method of regulation. Additionally, over more than a dozen imaging sessions, we did not observe any sustained interactions between NK cells and OT-I T cells in untreated or IL-15C–treated mice. Instead, we found that when IL-10Rα was removed from endothelial cells, the protective effect of IL-15C was substantially reduced in comparison to control mice.

Finally, we investigated how IL-15C treatment might act upon endothelial cells using a panel of surface markers associated with ECM. Over the past decade, the role of endothelial cell activation in CM pathology has become increasingly appreciated. Using confocal microscopy, we found that VCAM-1 expression is reduced upon $CD31^{+}$ vessels in response to IL-15C treatment. These results were confirmed by flow cytometry, with brain endothelial cell expression of both VCAM-1 and ICAM-1 reduced by treatment. We also tested whether antigen presentation by brain endothelial cells could be reduced with IL-15C treatment. Both $H\text{-}2K^{b}$ and $H\text{-}2D^{b}$ have been closely associated with ECM development,[8] and IL-15C treatment reduced the surface expression of both molecules on a per-cell basis. Importantly, we found that this reduction is dependent upon IL-10Rα expression on endothelial cells. Together, these data support a model in which IL-15C induces NK cell production of IL-10, thereby reducing the expression of adhesion molecules and MHC-I on brain endothelial cells and limiting CD8 T-cell arrest. Together, these data support a model in which the reduction in brain endothelial cell expression of adhesion and MHC-I molecules following IL-15C leads to reduced CD8 T-cell arrest, as observed in our thinned-skull window imaging experiments. Additional studies expanding this analysis and using technologies such as spatial transcriptomics will be impactful in understanding the role of endothelial cells in promoting or protecting against ECM.

IL-10 can have both positive and negative effects for malaria-infected hosts. Using a strain of *Plasmodium* that causes anemia but not CM in WT mice, $IL\text{-}10^{-/-}$ mice exerted superior control of parasitemia, but this came at the cost of developing CM-like disease.[56] Our work in PbA showed that when IL-10 is derived from NK cells, immunopathology is controlled, while parasite load is not impacted. While analysis of humans infected with malaria has relied on correlative studies, there is suggestive evidence that IL-10 can limit immunopathology. In one case study, high levels of circulating IL-10 cytokine were associated with decreased CM and renal failure, at the expense of parasite control.[57] This suggests that a balance of IL-10Rα expression is necessary to prevent tissue damage while still controlling parasite replication. We recently showed that NK cells from Malian adults express significantly higher levels of IL-10 than naïve US controls.[18] It remains to be seen how distinct cellular sources of IL-10 impact antimalarial immunity and other host functions. Additional studies are necessary to uncover how host sources of IL-10 may regulate immunity during human CM.

In summary, we show that treatment with IL-15C reduces the frequency of effector molecule expression by CD8 T cells in the brains of PbA-infected mice. We report that IL-15C treatment correlates with a reduced activation state of vascular endothelial cells in the brain, which may indirectly prevent CM development. Using multiphoton microscopy, we find that OT-I T-cell arrest is common in untreated mice experiencing ECM, and that this is reduced by IL-15C treatment. These data indicate that treatments delivered after infection that reduce CD8 T-cell arrest may be integral in preventing immunopathology-driven CM in the clinic.

Acknowledgments

We thank members of the Jameson and Hogquist laboratories for continuous feedback over the course of this study. We thank Dr. Stephen Jameson, Dr. Yoji Shimizu, Dr. Bryce Binstadt, and Dr. Eric Vivier for sharing mouse lines. We would also like to acknowledge members of the McGavern laboratory, who provided the training necessary for the thinned-skull window preparation that was used throughout this project. We acknowledge the following support services at the University of Minnesota that contributed to the research results reported: Research Animal Resources, University Flow Cytometry Resource, and the Center for Immunology Imaging Core. The authors acknowledge the late Shahid M. Khan (University of Leiden) for generating and characterizing the parasites used in this study.

Author contributions

Conceptualization: J.A.H. and S.E.H.; Methodology: J.A.H., G.T.H., and S.E.H.; Investigation: J.A.H. and E.D.L., with help from N.R.D., B.D.F., C.Y.K., J.A.S., J.S.M., and T.N.T.; Formal analysis: J.A.H., K.R.J., and J.S.M; Visualization: J.A.H.; Writing—original draft: J.A.H. and S.E.H.; Writing—review and editing: J.A.H., D.B.M., E.D.L., G.T.H., and S.E.H.; Funding acquisition: J.A.H., B.T.F., G.T.H, and S.E.H.; Resources: C.J.J., J.S.M., G.T.H., D.B.M., and B.T.F; Supervision: G.T.H. and S.E.H.

Jacob A. Hildebrand (Conceptualization [Equal], Formal analysis [Lead], Funding acquisition [Supporting], Investigation [Lead], Methodology [Lead], Visualization [Lead], Writing—original draft [Lead], Writing—review & editing [Equal]), Erin D. Lucas (Investigation [Supporting], Writing—review & editing [Equal]), Noah R. Daniels (Investigation [Supporting]), Benjamin D. Fisher (Investigation [Supporting]), Chris J. Janse (Resources [Equal]), Kory R. Johnson (Formal analysis [Supporting]), Caleb Y. Kim (Investigation [Supporting]), Jason S. Mitchell (Formal analysis [Supporting], Investigation [Supporting], Resources [Equal], Writing—review & editing [Equal]), Jules A. Sangala (Investigation [Supporting]), Trevor N. Tankersley (Investigation [Supporting]), Brian T. Fife (Funding acquisition [Supporting], Resources [Equal]), Dorian B. McGavern (Formal analysis [Supporting], Resources [Equal], Writing—review & editing [Equal]), Geoffrey T. Hart (Funding acquisition [Supporting], Methodology [Equal], Resources [Equal], Supervision [Equal], Writing—review & editing [Equal]), and Sara E. Hamilton (Conceptualization [Equal], Funding acquisition [Lead], Methodology [Equal], Project administration [Lead], Supervision [Lead], Writing—original draft [Equal], Writing—review & editing [Equal])

Supplementary material

Supplementary material is available at *The Journal of Immunology* online.

Funding

This research was supported by the following funding sources: National Institutes of Health (NIH)/National Institute of Allergy and Infectious Diseases (NIAID) R01AI143828 (S.E.H.), NIH/NIAID T32AI007313 (J.A.H.), and the NIH/National Institute of Neurological Disorders and Stroke (NINDS) intramural program. Multiphoton and confocal imaging on the Leica Stellaris 8 DIVE system was made possible by an NIH S10 grant 1S10OD034456-01 (B.T.F.) in the University of Minnesota Center for Immunology.

Conflicts of interest

All authors declare that they have no competing interests.

Data availability

All data supporting the findings of this study are available upon request to the corresponding authors. The raw data used for generating graphs in this manuscript are provided in the Source Data file.

References

1. World Health Organization. World malaria report 2025: addressing the threat of antimalarial drug resistance. World Health Organization; 2025. https://www.who.int/teams/global-malaria-programme/reports/world-malaria-report-2025
2. Albrecht-Schgoer K, Lackner P, Schmutzhard E, Baier G. Cerebral malaria: current clinical and immunological aspects. Front Immunol. 2022;13:863568. https://doi.org/10.3389/fimmu.2022.863568
3. World Health Organization. Guidelines for the treatment of malaria. 3rd ed. World Health Organization; 2015. https://iris.who.int/handle/10665/162441
4. Wicht KJ, Mok S, Fidock DA. Molecular mechanisms of drug resistance in *Plasmodium falciparum* malaria. Ann Rev Microbiol. 2020;74:431–454. https://doi.org/10.1146/annurev-micro-020518-115546
5. Nishanth G, Schlüter D. Blood-brain barrier in cerebral malaria: pathogenesis and therapeutic intervention. Trends Parasitol. 2019;35:516–528. https://doi.org/10.1016/j.pt.2019.04.010
6. Howland SW et al. Brain microvessel cross-presentation is a hallmark of experimental cerebral malaria. EMBO Mol Med. 2013;5:984–999. https://doi.org/10.1002/emmm.201202273
7. Swanson PA II, et al. CD8+ T cells induce fatal brainstem pathology during cerebral malaria via luminal antigen-specific engagement of brain vasculature. PLoS Pathog. 2016;12:e1006022. https://doi.org/10.1371/journal.ppat.1006022
8. Fain CE et al. Discrete class I molecules on brain endothelium differentially regulate neuropathology in experimental cerebral malaria. Brain J Neurol. 2024;147:566–589. https://doi.org/10.1093/brain/awad319
9. Belnoue E et al. Control of pathogenic CD8+ T cell migration to the brain by IFN-γ during experimental cerebral malaria. Parasite Immunol. 2008;30:544–553. https://doi.org/10.1111/j.1365-3024.2008.01053.x
10. Huggins MA et al. Perforin expression by CD8 T cells is sufficient to cause fatal brain edema during experimental cerebral malaria. Infect Immun. 2017;85:e00985-16. https://doi.org/10.1128/IAI.00985-16

11. Potter S et al. Perforin mediated apoptosis of cerebral microvascular endothelial cells during experimental cerebral malaria. Int J Parasitol. 2006;36:485–496. https://doi.org/10.1016/j.ijpara.2005.12.005
12. Haque A et al. Granzyme B expression by CD8+ T cells is required for the development of experimental cerebral malaria. J Immunol. 2011;186:6148–6156. https://doi.org/10.4049/jimmunol.1003955
13. Riggle BA et al. CD8+ T cells target cerebrovasculature in children with cerebral malaria. J Clin Invest. 2020;130:1128–1138. https://doi.org/10.1172/JCI133474
14. Ljunggren HG, Kärre K. In search of the "missing self": MHC molecules and NK cell recognition. Immunol Today. 1990;11:237–244. https://doi.org/10.1016/0167-5699(90)90097-s
15. Crouse J, Xu HC, Lang PA, Oxenius A. NK cells regulating T cell responses: mechanisms and outcome. Trends Immunol. 2015;36:49–58. https://doi.org/10.1016/j.it.2014.11.001
16. Pallmer K, Oxenius A. Recognition and regulation of T cells by NK cells. Front Immunol. 2016;7:251. https://doi.org/10.3389/fimmu.2016.00251
17. Burrack KS et al. Interleukin-15 complex treatment protects mice from cerebral malaria by inducing interleukin-10-producing natural killer cells. Immunity. 2018;48:760–772.e4. https://doi.org/10.1016/j.immuni.2018.03.012
18. McNitt SA et al. Phenotype and function of IL-10–producing NK cells in individuals with malaria experience. JCI Insight. 2025;10:e183076. https://doi.org/10.1172/jci.insight.183076
19. Hogquist KA et al. T cell receptor antagonist peptides induce positive selection. Cell. 1994;76:17–27. https://doi.org/10.1016/0092-8674(94)90169-4
20. Shen FW et al. Cloning of Ly-5 cDNA. Proc Natl Acad Sci U S A. 1985;82:7360–7363. https://doi.org/10.1073/pnas.82.21.7360
21. Schaefer BC, Schaefer ML, Kappler JW, Marrack P, Kedl RM. Observation of antigen-dependent CD8+ T-cell/dendritic cell interactions in vivo. Cell Immunol. 2001;214:110–122. https://doi.org/10.1006/cimm.2001.1895
22. Okabe K et al. Neurons limit angiogenesis by titrating VEGF in retina. Cell. 2014;159:584–596. https://doi.org/10.1016/j.cell.2014.09.025
23. Narni-Mancinelli E et al. Fate mapping analysis of lymphoid cells expressing the NKp46 cell surface receptor. Proc Natl Acad Sci U S A. 2011;108:18324–18329. https://doi.org/10.1073/pnas.1112064108
24. Madisen L et al. A robust and high-throughput Cre reporting and characterization system for the whole mouse brain. Nat Neurosci. 2010;13:133–140. https://doi.org/10.1038/nn.2467
25. Maekawa Y et al. Notch2 integrates signaling by the transcription factors RBP-J and CREB1 to promote T cell cytotoxicity. Nat Immunol. 2008;9:1140–1147. https://doi.org/10.1038/ni.1649
26. Liu X et al. The T cell response to IL-10 alters cellular dynamics and paradoxically promotes central nervous system autoimmunity. J Immunol. 2012;189:669–678. https://doi.org/10.4049/jimmunol.1200607
27. Killick-Kendrick R. Parasitic protozoa of the blood of rodents: a revision of *Plasmodium berghei*. Parasitology. 1974;69:225–237. https://doi.org/10.1017/S0031182000048071
28. Lin J-W et al. The subcellular location of ovalbumin in plasmodium berghei blood stages influences the magnitude of T-cell responses. Infect Immun. 2014;82:4654–4665. https://doi.org/10.1128/IAI.01940-14
29. Hildebrand JA et al. Severe malaria enforces short-lived effector cell differentiation but does not prevent effective secondary responses by memory CD8 T cells. PLoS Pathog. 2025;21:e1012993. https://doi.org/10.1371/journal.ppat.1012993
30. Shelton SB et al. A simple, efficient tool for assessment of mice after unilateral cortex injury. J Neurosci Methods. 2008;168:431–442. https://doi.org/10.1016/j.jneumeth.2007.11.003
31. Anderson KG et al. Intravascular staining for discrimination of vascular and tissue leukocytes. Nat Protoc. 2014;9:209–222. https://doi.org/10.1038/nprot.2014.005
32. Lauterbach H, Zuniga EI, Truong P, Oldstone MBA, McGavern DB. Adoptive immunotherapy induces CNS dendritic cell recruitment and antigen presentation during clearance of a persistent viral infection. J Exp Med. 2006;203:1963–1975. https://doi.org/10.1084/jem.20060039
33. Manglani M, McGavern DB. Intravital imaging of neuroimmune interactions through a thinned skull. Curr Protoc Immunol. 2018;120:24.2.1-24.2.12. https://doi.org/10.1002/cpim.46
34. Joshi NS et al. Inflammation directs memory precursor and short-lived effector CD8(+) T cell fates via the graded expression of T-bet transcription factor. Immunity. 2007;27:281–295. https://doi.org/10.1016/j.immuni.2007.07.010
35. Paul D, Cowan AE, Ge S, Pachter JS. Novel 3D analysis of Claudin-5 reveals significant endothelial heterogeneity among CNS microvessels. Microvasc Res. 2013;86:1–10. https://doi.org/10.1016/j.mvr.2012.12.001
36. Qin J et al. Perivascular macrophages create an intravascular niche for CD8+ T cell localisation prior to the onset of fatal experimental cerebral malaria. Clin Transl Immunol. 2021;10:e1273. https://doi.org/10.1002/cti2.1273
37. Howland SW, Poh CM, Rénia L. Activated brain endothelial cells cross-present malaria antigen. PLoS Pathog. 2015;11:e1004963. https://doi.org/10.1371/journal.ppat.1004963
38. Claser C et al. Lung endothelial cell antigen cross-presentation to CD8+ T cells drives malaria-associated lung injury. Nat Commun. 2019;10:4241. https://doi.org/10.1038/s41467-019-12017-8
39. Gleissner CA et al. IL-10 inhibits endothelium-dependent T cell costimulation by up-regulation of ILT3/4 in human vascular endothelial cells. Eur J Immunol. 2007;37:177–192. https://doi.org/10.1002/eji.200636498
40. Vora M, Yssel H, de Vries JE, Karasek MA. Antigen presentation by human dermal microvascular endothelial cells. Immunoregulatory effect of IFN-gamma and IL-10. J Immunol. 1994;152:5734–5741. https://doi.org/10.4049/jimmunol.152.12.5734
41. Linares M et al. Brain-derived neurotrophic factor and the course of experimental cerebral malaria. Brain Res. 2013;1490:210–224. https://doi.org/10.1016/j.brainres.2012.10.040
42. Bauer PR, Van Der Heyde HC, Sun G, Specian RD, Granger DN. Regulation of endothelial cell adhesion molecule expression in an experimental model of cerebral malaria. Microcirculation. 2002;9:463–470. https://doi.org/10.1038/sj.mn.7800159
43. Chang W-L et al. P-selectin contributes to severe experimental malaria but is not required for leukocyte adhesion to brain microvasculature. Infect Immun. 2003;71:1911–1918. https://doi.org/10.1128/IAI.71.4.1911-1918.2003

44. Combes V et al. Pathogenic role of P-selectin in experimental cerebral malaria: importance of the endothelial compartment. Am J Pathol. 2004;164:781–786. https://doi.org/10.1016/S0002-9440(10)63166-5
45. Turner L et al. Severe malaria is associated with parasite binding to endothelial protein C receptor. Nature. 2013;498:502–505. https://doi.org/10.1038/nature12216
46. Dos Santos Ortolan L et al. Endothelial protein C receptor could contribute to experimental malaria-associated acute respiratory distress syndrome. J Immunol Res. 2019;2019:3105817. https://doi.org/10.1155/2019/3105817
47. Sharma S et al. A pathogenic role for IL-10 signalling in capillary stalling and cognitive impairment in type 1 diabetes. Nat Metab. 2024;6:2082–2099. https://doi.org/10.1038/s42255-024-01159-9
48. Bensalel J, Gallego-Delgado J. Exploring adjunctive therapies for cerebral malaria. Front Cell Infect Microbiol. 2024;14:1347486. https://doi.org/10.3389/fcimb.2024.1347486
49. Howard JN, Bosque A. IL-15 and N-803 for HIV cure approaches. Viruses. 2023;15:1912. https://doi.org/10.3390/v15091912
50. Leidner R et al. First-in-human phase I/Ib study of NIZ985, a recombinant heterodimer of IL-15 and IL-15Rα, as a single agent and in combination with spartalizumab in patients with advanced and metastatic solid tumors. J Immunother Cancer. 2023;11:e007725. https://doi.org/10.1136/jitc-2023-007725
51. Guo Y, Luan L, Patil NK, Sherwood ER. Immunobiology of the IL-15/IL-15Rα complex as an antitumor and antiviral agent. Cytokine Growth Factor Rev. 2017;38:10–21. https://doi.org/10.1016/j.cytogfr.2017.08.002
52. Salmela K et al. A randomized multicenter trial of the anti-icam-1 monoclonal antibody (enlimomab) for the prevention of acute rejection and delayed onset of graft function in cadaveric renal transplantation: a report of the European Anti-ICAM-1 Renal Transplant Study Group. Transplantation. 1999;67:729–736. https://doi.org/10.1097/00007890-199903150-00015
53. Vincenti F et al. A phase I/II randomized open-label multicenter trial of efalizumab, a humanized anti-CD11a, anti-LFA-1 in renal transplantation. Am J Transplant. 2007;7:1770–1777. https://doi.org/10.1111/j.1600-6143.2007.01845.x
54. Pickett JR, Wu Y, Zacchi LF, Ta HT. Targeting endothelial vascular cell adhesion molecule-1 in atherosclerosis: drug discovery and development of vascular cell adhesion molecule-1–directed novel therapeutics. Cardiovasc Res. 2023;119:2278–2293. https://doi.org/10.1093/cvr/cvad130
55. Favre N et al. Role of ICAM-1 (CD54) in the development of murine cerebral malaria. Microbes Infect. 1999;1:961–968. https://doi.org/10.1016/S1286-4579(99)80513-9
56. Sanni LA, Jarra W, Li C, Langhorne J. Cerebral edema and cerebral hemorrhages in interleukin-10-deficient mice infected with *Plasmodium chabaudi*. Infect Immun. 2004;72:3054–3058. https://doi.org/10.1128/IAI.72.5.3054-3058.2004
57. Day NP et al. The prognostic and pathophysiologic role of pro- and antiinflammatory cytokines in severe malaria. J Infect Dis. 1999;180:1288–1297. https://doi.org/10.1086/315016

© The Author(s) 2026. Published by Oxford University Press on behalf of The American Association of Immunologists.
This is an Open Access article distributed under the terms of the Creative Commons Attribution-NonCommercial License (https://creativecommons.org/licenses/by-nc/4.0/), which permits non-commercial re-use, distribution, and reproduction in any medium, provided the original work is properly cited. For commercial re-use, please contact reprints@oup.com for reprints and translation rights for reprints. All other permissions can be obtained through our RightsLink service via the Permissions link on the article page on our site—for further information please contact journals.permissions@oup.com.
The Journal of Immunology, 2026, 215, 1–15
https://doi.org/10.1093/jimmun/vkag295
Cutting Edge